Process Safety and Environmental Protection 183 (2024) 260–273

Contents lists available at ScienceDirect

Process Safety and Environmental Protection

journal homepage: www.journals.elsevier.com/process-safety-and-environmental-protection

Enhancing fire safety in underground mines: Experimental and large eddy simulation of temperature attenuation, gas evolution, and bifurcation influence for improved emergency response

Oluwafemi B. Salami [a], Ashish Ranjan Kumar [b], Iqbal Aamir [a], Robert Ilango Pushparaj [a], Guang Xu [a,*]

[a] Department of Mining and Explosives Engineering, Missouri University of Science and Technology, Rolla, MO, 65401, USA
[b] Department of Energy and Mineral Engineering, Penn State University Park, PA 16802, USA

ARTICLE INFO

Keywords:
Full-scale fire
Temperature attenuation
Buoyancy-driven flow
Underground space bifurcation
Emergency evacuation

ABSTRACT

The occurrence of underground mine fires remains a significant and persistent safety challenge in the mining industry, posing imminent risks to both miners' lives and the operational integrity of mining facilities. Current underground mine fire studies lack scale accuracy due to lab experiments and fail to consider bifurcation effects on smoke gas temperature. This study performed full-scale experiments and built validated CFD models to explore the interactive impact of ventilation and fire size on temperature attenuation, gas behavior, and CO generation in underground mines. A new empirical correlation for temperature decay in the mine drift was developed and its accuracy was compared with established models in the literature. In addition, the influence of bifurcation on maximum smoke temperature was analyzed. This research combines full-scale experiments and validated CFD modeling to address major gaps in underground mine fire studies. Unlike previous methods, this study explores the interactive effects of ventilation, fire size, temperature attenuation, and toxic gas spread, offering unprecedented insights. This innovation enables the development of tailored fire safety standards for mines, ensuring safer designs, rapid fire suppression, and improved evacuation strategies. By bridging theory and practice, this work transforms fundamental knowledge, empowering the mining industry to enhance safety measures, protect lives, and mitigate the impact of underground mine fires.

1. Introduction

Fires in underground confined spaces are extremely dangerous and remains one of the most catastrophic environmental hazards that may occur in mines (Chen et al., 2023; Fernández-Alaiz et al., 2020; Huang et al., 2022; Kamran et al., 2023; Khan and Abbasi, 1999; Lei et al., 2021; Mavhura, 2019; Salami et al., 2023a; Wang et al., 2022; Xiang et al., 2021; Yuan et al., 2018). Studies have shown that mine fires produce high levels of toxic gases and smoke which could be dispersed quickly through the ventilation network to various parts of the underground workings (Düzgün and Leveson, 2018; Iqbal et al., 2023; Kamran et al., 2023; Salami and Xu, 2022; Salami et al., 2023a). The toxic smoke released during fires further reduce visibility and escape chances of trapped occupants during fires (Chen et al., 2023; Kirytopoulos et al., 2014; Lee and Ghazali, 2018; Lei et al., 2021). Most fatalities due to underground fires could be attributed to the inhalation of noxious smoke gases mainly carbon monoxide (Bahrami et al., 2021; Chen et al., 2023; Zhou, 2009; Zhou et al., 2018).

Quantifying fire development is critical to developing improved industrial fire safety measures such as predicting the fire development trends, evaluating the severity of the accidents, assessing the losses due to fires in real-time and informing the fire fighting and emergency response tactics (Huang et al., 2022; Salami and Xu, 2022; Salami et al., 2023b; Yuan et al., 2018). Presently, underground mine fire hazard quantification, fire risk assessment, and risk mitigation studies have employed various approaches ranging from small scale experiments, full-scale tests, and numerical methods such as computational fluid dynamics (CFD) (Hansen and Ingason, 2013a; Ingason and Li, 2010; Li et al., 2011; Lu et al., 2022; Oka and Atkinson, 1995; Yuan et al., 2016).

Several studies have been conducted using experimental and numerical techniques on mine fire detection, suppression, and firefighting (Lei et al., 2021; Yuan et al., 2018). Liu et al. (Liu et al., 2017)

* Corresponding author.
E-mail address: xuguang@vt.edu (G. Xu).

https://doi.org/10.1016/j.psep.2023.12.056
Received 22 October 2023; Received in revised form 16 December 2023; Accepted 23 December 2023
Available online 30 December 2023

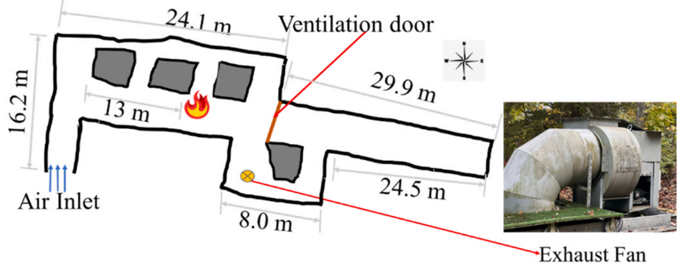

Fig. 1. Plan view of the study location and the exhaust fan.

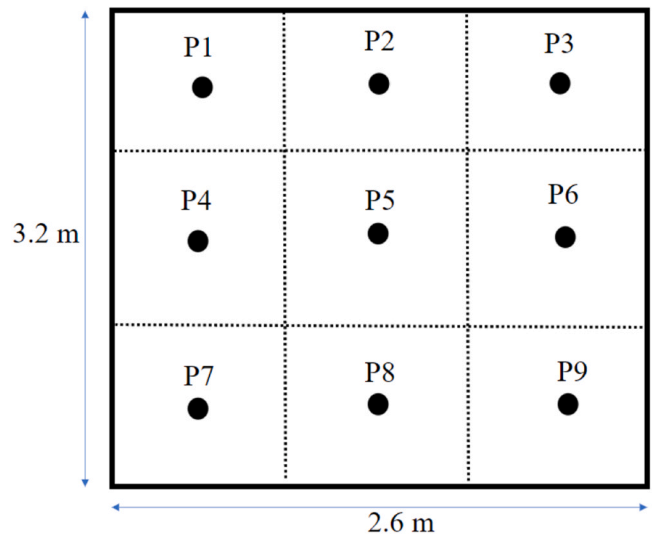

Fig. 2. Velocity measuring points at the station's cross Section 3m downstream of fire.

established a new temperature decay model due to fire-induced smoke in an underground mine. Hong et al. (Hong et al., 2022) used a combination of different machine models to predict the spread of smoke of fire smoke in mine tunnels. The study demonstrated that ML models such as random forest (RF), support vector machine (SVM), and artificial neural network could predict whether back flow of fire smoke will occur or not. Dong et al. (Dong et al., 2017) investigated the effectiveness of aqueous form for fire-fighting in underground and discovered that foam could block the cracks in coal goaf thus preventing the supply of air to the goaf and subsequent oxidation which may lead to fire. In another study, Chen et al. (Chen et al., 2023) conducted studies that allow the design of a fire protection system for tunnel fires. The effect of centralized ceiling smoke exhaust system with air curtains were examined with plug-holing phenomenon during a tunnel fire and a new predictive model that could forecast the smoke exhaust efficiency for the coupled system with a fire size of up to 20 MW was developed.

In addition, some studies have also investigated the heat release of mining vehicles in a full-scale fire test by burning mining trucks in an underground mine (Hansen, 2019; Hansen and Ingason, 2013b, 2013c). Whereas, many other researchers have employed numerical approaches such as CFD and ventilation network analysis models to complement full-scale fire experiments (Gannouni and Maad, 2015; Haghighat et al., 2018; Yuan and Smith, 2015; Yuan et al., 2016; Zhu et al., 2016). This is due to the high cost of conducting full-scale tests, and sometimes to examine fires that are too dangerous or expensive to effectuate in real-world settings (Salami et al., 2023a).

CFD has been successfully applied to evaluate fires hazards, fire suppression performances, and smoke and gases dispersion in mining related problems (Chang et al., 2019; Fernández-Alaiz et al., 2020; Salami et al., 2023a; Xu et al., 2016; Yuan and Smith, 2015). In a series of studies, full-scale tests and analogous CFD simulations were deployed to examine the ventilation influence on mine fire evolution (Fernández-Alaiz et al., 2020a; Fernández-Alaiz et al., 2020b; Fernánez-Alaiz et al., 2020c). Findings from the CFD simulations were extended to examine the hazards of potential fire occurrence and the effectiveness of available emergency response in the mine (Fernández-Alaiz, 2020a). The study highlighted important trends of the fire based on the ventilation-fuel load ratio, thus successfully predicting the potential impact of fires within the underground space. In another research, a CFD model was developed to evaluate the effect of sprinkler activation temperature, water flow rate, and the location of the sprinkler on the suppression of conveyor belts fires in mines (Yuan and Smith, 2015).

Presently, our understanding about fires and toxic gases spread in underground mines are inadequate to develop appropriate fire risk assessment framework for underground mining environments. First, most of the existing fire risk management studies were conducted using a model-scale tunnel apparatus in the laboratory which makes it impossible to preserve all the dimensionless terms derived by the scaling theory (Li and Ingason, 2012; Salami et al., 2023a). Secondly, findings from existing literature have failed to account for the influence of bifurcations on the maximum smoke gas temperature beneath the ceiling in an underground mine, as compared to transport tunnels. The generation of carbon monoxide (CO)-a chief cause of miners' fatalities in the underground – is also been neglected in most mine/tunnel fire studies (Han et al., 2021; Huang et al., 2018; Li and Ingason, 2012; Li et al., 2011; Tang et al., 2018; Zhang et al., 2021).

Another major concern is that accidents continue to occur despite the tremendous progress that has been made regarding the risk assessment frameworks and due to the complex nature of underground environments (Gehandler, 2015). Therefore, it remains unclear whether applying risk assessment method is capable of ensuring sufficient preparedness against a fire occurrence (Ntzeremes and Kirytopoulos, 2019). To address this shortcoming, it important to employ a combination of full-scale experimental and numerical techniques that will enhance our understanding of the fire and smoke spread mechanism, and the influence of bifurcation on maximum smoke gas temperature induced by fire in underground mines.

The objective of this study is to investigate the interactive influence of ventilation and fire size on temperature attenuation, maximum excess gas temperature, and toxic gas spread using full-scale experiments. A CFD model was built and validated based on the experimental scenario, and the model was extended to investigate the influence of bifurcations on maximum excess smoke gas temperature due to fire-induced smoke flow in the underground mine. A new empirical correlation for temperature decay in the mine drift was developed and the accuracy analyzed by comparing the new model with existing models. The influence of fire size and ventilation conditions on the generation of carbon monoxide (CO) in the mine was also analyzed using the peak value of CO emitted during each fire test. The importance of this study is to aid the development of new fire safety standards and suppression techniques. This research would serve a reliable guide for estimating the fire intensity and assessing the risk of fires in deep underground environments and would aid a safe, and environmentally friendly fire risk management in the future design of subsurface environments. The data obtained from this study will be very useful to validate existing mine fire CFD models, thus improving the safe application of emergency evacuation strategies in the event of an underground fire.

2. Experimental methods

2.1. Test location

The Missouri S&T experimental mine was used for this investigation. The layout of the mine is presented in Fig. 1. The mine airways are approximately rectangular in shape with an average width of 2.6 m and

Table 1
Randomized experimental test cases.

Experiment	1	2	3	4	5	6	7	8	9
Ventilation rate (%)	100	50	0	0	50	50	100	100	0
Exhaust Air Volume (m^3/s)	5.42	2.97	0.24	0.24	2.97	2.97	5.42	5.42	0.24
Fire Size (m)	0.7	0.5	0.5	0.7	0.7	0.3	0.3	0.5	0.3
Ambient Temperature (°C)	27.5	22.5	22.5	22.5	19.5	19.5	19.5	19.5	19.5

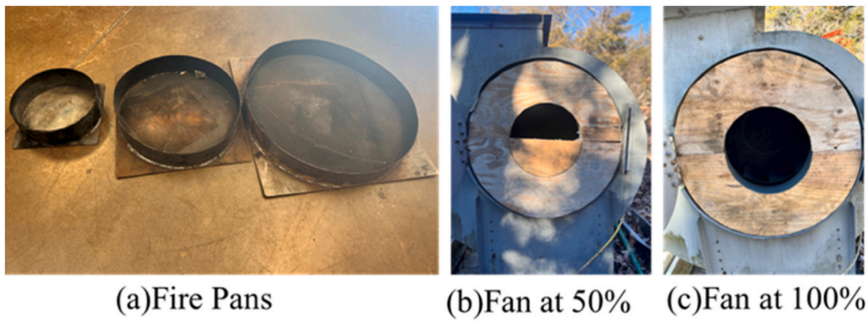

Fig. 3. Fire pans and the fan opening.

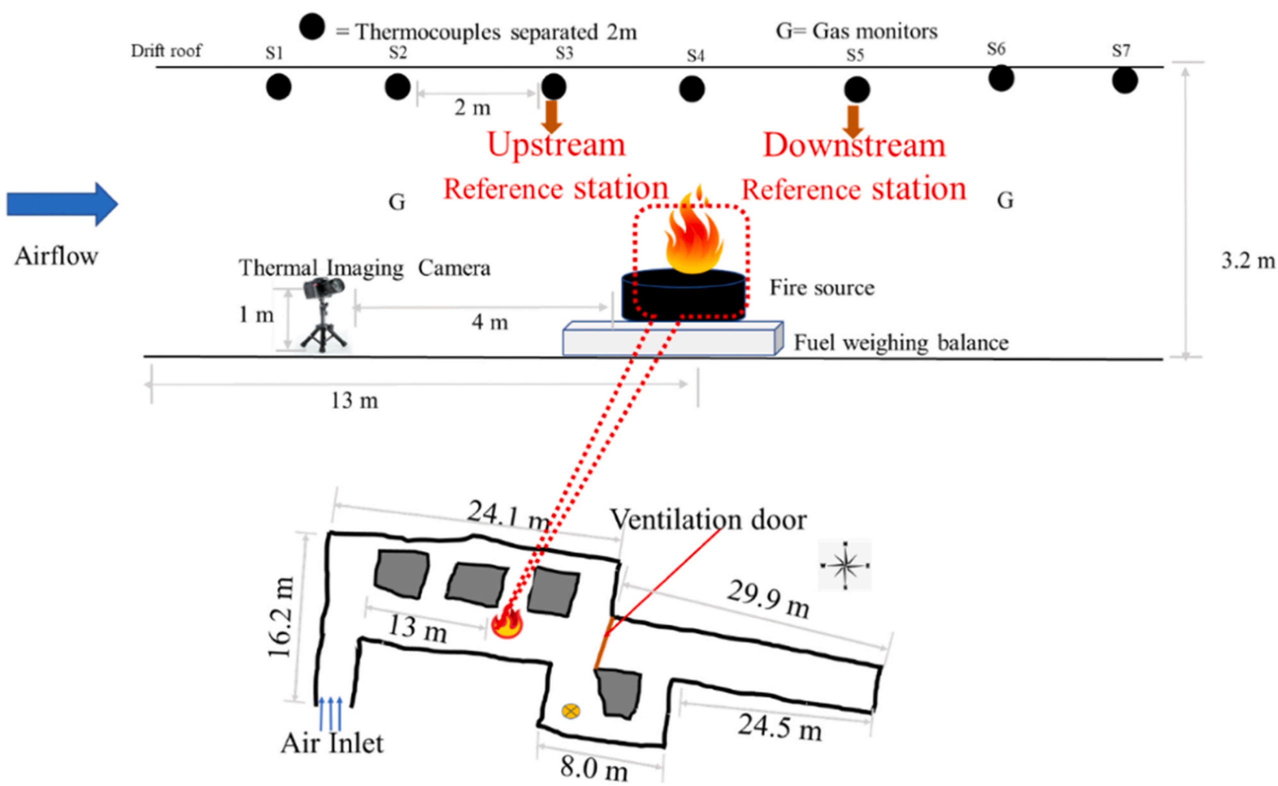

Fig. 4. Complete experimental instrumentation.

height of 3.2 m. The mine is a typical room-and-pillar underground mine with four pillars and a main drift about 54 m long. Air enters the mine from the entrance at the lower part of the map in Fig. 1, and was exhausted through a ventilation fan on the surface.

2.2. Full scale fire test

The weighing scale was first set up and the fire pan was then placed on a 30 cm by 30 cm frame to avoid direct contact with the scale since the elevated temperature may destroy the scale. Secondly, the scale was tarred to zero before the diesel was poured into the pan to get precise weight of the fuel. The monitors and sensors were then synchronized to log the data from a remote computer before the fire pool was ignited.

Longitudinal ventilation velocity in the mine was determined 3 m downstream of the fire location using the point transverse method before each fire pool test. The fire pool was placed at 13 m from the in-by portal along the main drift (indicated by a fire icon in Fig. 1). The points traverse measurements were conducted using a rotating vane electrical anemometer. The measurement was done by dividing the cross section into nine equal rectangle area and measuring the velocity at

Fig. 5. Sample image from TIC taken during the experiment.

center points for 30 s before taking the average reading of the anemometer. The measuring point along the cross-section is denoted as P1 to P9 as shown in Fig. 2.

Two factors: The fire pool size and ventilation rate were used for the experimental design: each factor had three levels and a total of nine experimental runs were conducted using a 3^k factorial design. The factors and the measured ambient temperature are presented in Table 1.

Pool containers of diameter 0.3 m, 0.5 m, and 0.7 m, as shown in Fig. 3(a), were used for this investigation, while longitudinal ventilation conditions were varied by adjusting the ceiling smoke extraction rate between 0–100%. 0% ventilation implies the exhaust fan was put off, the 50% ventilation is achieved by turning the fan on but blocking half of the fan duct cross-section area using a circular wooden board as shown in Fig. 3(b) while 100% ventilation is achieved when the fan duct is completely opened as depicted in Fig. 3(c).

For each of the fire test, 0.5 gal of diesel was used. After each test, 10 mins were allowed with the fan fully operational to exhaust the smoke and allow the underground temperature to reset to near ambient conditions for the subsequent experimentats. The mine had a ventilation door located at approximately 12 m from the fire pool downstream which separated the testing region from the blind heading of the main drift in the underground. Thus, the fire could be considered axisymmetric within the test region. CO monitors (EasyLog CO monitors), denoted as "G" in Fig. 4, were placed 4 m upstream and downstream of the fire and 1.5 m above the floor to measure the carbon monoxide concentration. Smoke temperature was measured beneath the mine ceiling, and at position 1 m below the roof of the mine using K-type thermocouples. At the roof of the mine, thermocouples were installed at all seven locations (S1-S7), as depicted in Fig. 4, whereas thermocouples could only be installed at stations S1, S2, S3, S5, S6, and S7 1 m below the roof of the mine. No thermocouple was installed at S6 because it was too close to the fire surface and could be destroyed quickly by the fire.

Additionally, a thermal imaging camera (TIC) was mounted 4 m upstream of fire during the tests. The TIC was utilized to capture the surface temperature of the fire for the post fire analysis of the fire flame properties. A sample of the image from the TIC taken during the experiment is shown in Fig. 5.

2.3. Heat release rate (HRR) determination

The heat release rate is the most important fire parameter. It is also a very critical input for CFD simulations of fire. The HRR was used to estimate the fire intensity. It can be determined by measuring the changes in the mass of the fuel to the burning time, as given in Eq. (1) (Yuan et al., 2016; Zhou et al., 2018):

$$Q = m^{'}\Delta H_c \tag{1}$$

where $m^{'}$ is the burning rate or mass loss rate (kgs^{-1}), and ΔH_c is the heat of combustion ($kJ.kg^{-1}$).

2.4. Thermal image and flame analysis

The flame analysis was done using the FLIR E 86 Thermal Imaging Camera (TIC). The FLIR E 86 was embedded with high performance features required for quick and accurate detection of hot spots. The TIC has a 464 × 348 pixel and an expanded temperature range for accurate temperature detection. However, the temperature range of 0–650 °C was selected for this study. The purpose of analyzing the flame was to identify high-risk zones to fire rescuers and emergency responders for a given fire scenario, thereby improving fire safety. The TIC images were analyzed using the image segmentation toolbox in MATLAB, which was achieved by following the basics steps: (1) identifying elevated temperature spots (2) extracting the temperature values at the marked spot (3) plotting temperature values at the marked spot (4) obtaining maximum temperature values for the marked regions.

3. Numerical simulations

3.1. Computational domain

The grid size used for a CFD- fire dynamic simulation (FDS) is the principal factor that determines the resolution of the FDS simulation. It could impact properties like fire smoke temperature measured at the underground ceiling. For this reason, appropriate grid sensitivity should be done to obtain mesh independence. In FDS, the grid size can be derived from the fire characteristic diameter given in Eq. (2) (McGrattan et al., 2013; Weng et al., 2015):

$$D^{*} = \left(\frac{\dot{Q}}{\rho_{\infty} c_p T_{\infty}\sqrt{g}}\right)^{2/5} \tag{2}$$

where δx denotes the nominal size of the mesh cell, $\dot{Q}$ represents the total heat release rate of the fire (kW), ρ_{∞} designates the ambient air density

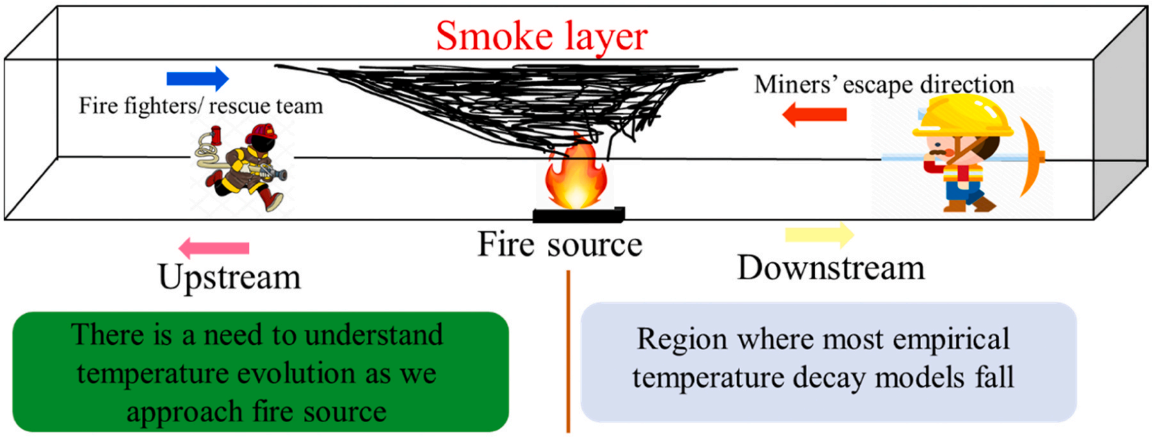

Fig. 6. Illustration of region of applicability of existing temperature attenuation models.

Table 2
Point traverse airflow 3 m downstream of fire.

S/N	P1	P2	P3	P4	P5	P6	P7	P8	P9
Exp 1	0.47	0.33	0.27	0.32	0.12	0.00	0.33	0.16	0.04
Exp 2	0.16	0.16	0.21	0.00	0.00	0.07	0.07	0.11	0.06
Exp 3	0.00	0.00	0.00	0.00	0.00	0.00	0.07	0.00	0.04
Exp 4	0.00	0.00	0.00	0.00	0.00	0.00	0.07	0.00	0.04
Exp 5	0.16	0.16	0.21	0.00	0.00	0.07	0.07	0.11	0.06
Exp 6	0.16	0.16	0.21	0.00	0.00	0.07	0.07	0.11	0.06
Exp 7	0.47	0.33	0.27	0.32	0.12	0.00	0.33	0.16	0.04
Exp 8	0.47	0.33	0.27	0.32	0.12	0.00	0.33	0.16	0.04
Exp 9	0.00	0.00	0.00	0.00	0.00	0.00	0.07	0.00	0.04

Table 3
Heat release rate values obtained for the experimental cases.

S/N	Test Case	Pool diameter (m)	Ventilation Opening (%)	HRR (KW)
1	Exp 4	0.7	0	425
2	Exp 5	0.7	50	425
3	Exp 1	0.7	100	425
4	Exp 3	0.5	0	212.5
5	Exp 2	0.5	50	212.5
6	Exp 8	0.5	100	212.5
7	Exp 9	0.3	0	85
8	Exp 6	0.3	50	85
9	Exp 7	0.3	100	85

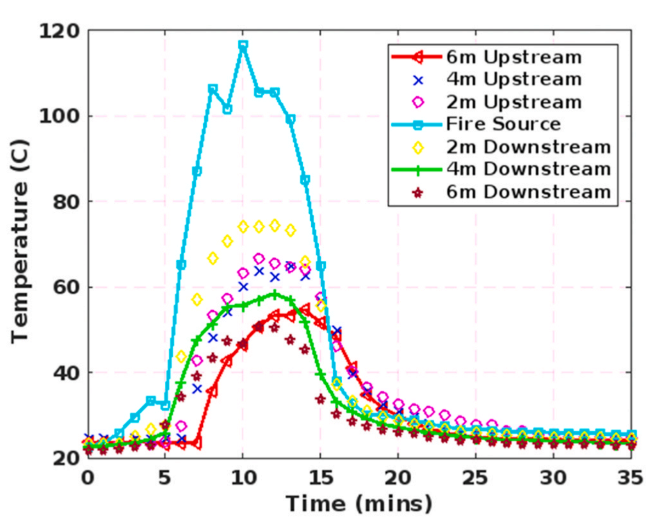

Fig. 7. Temperature curves measured at different distances for Test 2.

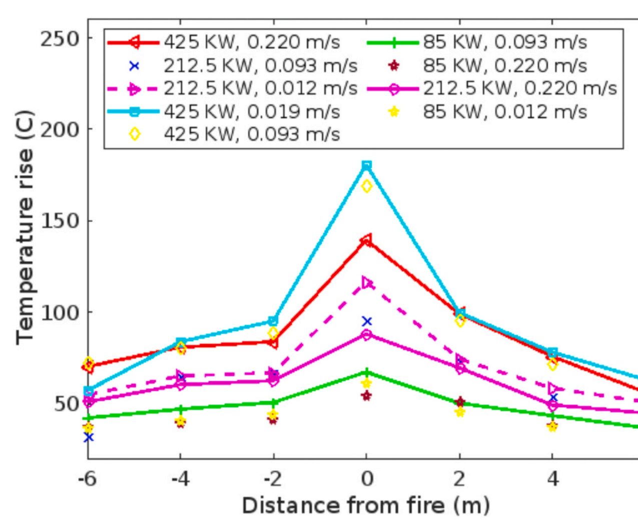

Fig. 8. Maximum rise in smoke temperature at the mine roof for the different ventilation conditions.

kg/m^3, C_p is the specific heat capacity of air (KJ/kg/k), T_∞ is the ambient temperature (K), and g is the acceleration due to gravity (usually taken as 9.81 m/s^2) (McGrattan et al., 2013; McGrattan et al., 2016; Overholt, 2014).

The ratio of the fire characteristic size to grid size ($D^*/\delta x$), known as the plume resolution (PR) index, is normally used to describe the quality of the calculation grid (Gannouni and Maad, 2015). The higher this value is, the finer the meshes are and the more computational time will be required for the CFD simulation. However, sensitivity studies from the literature have recommended that values between 4 to 16 are sufficient to obtain an appropriate resolution with minimal computational

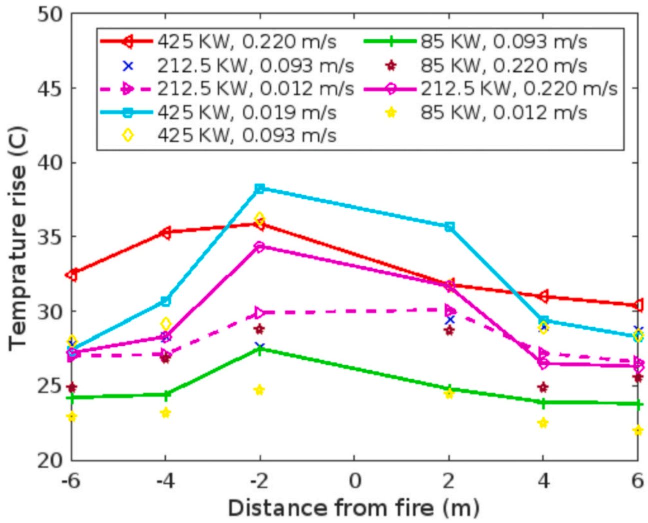

Fig. 9. Maximum rise in smoke temperature 1 m below the mine roof for the different ventilation conditions.

requirements (McGrattan et al., 2013; McGrattan et al., 2014). The mesh size for this simulation is also determined by this rule. For this study, the computational domain was obtained by setting the x, $x^{'}$, y, $y^{'}$, z, and $z^{'}$ to 0, 54, 0, 12.5, and 0, 3.2 where x, y, and z represent the minimum values and $x^{'}$, $y^{'}$, *andz*$^{'}$ denote the maximum values for the coordinates x, y, and z, respectively.

The mesh size for this simulation was determined based on the experimental case considered before the model was validated. The experimental case examined was 0.7 m diameter pool fire with a 100% smoke ceiling extraction. The maximum HRR of the fire obtained from the experiment was 425.0 KW. The computed characteristics fire diameter, D^{*}, was 4.91. Based on the calculated fire characteristics diameter, a mesh size of 0.2 m was selected to obtain adequate mesh size for the grid calculations.

3.2. Simulation parameters and boundary conditions

For this study, the default setting for the dynamic turbulence modeling was retained. The default settings adopted the constant Smagorinsky model (where $P_{rt} = 0.5$, $S_{ct} = 0.5$, $andC_s$=0.17). Furthermore, the environmental conditions were set to the experimental conditions during the fire test. The HRRPUA for the FDS simulation was set based on 425 KW fire and the calculated pool area. The reaction type was set as "HEPTANE'', "CO_YIELD = 0.1", and the "SOOT_YIELD = 0.1". The main inlet to the mine was modeled as "OPEN" surface. Similarly, the exhaust fan was modeled as "EXHASUT" with a specified volume flow of 5.42 m^3/s. Furthermore, the pillars were modeled as a slab obstruction, the materials for the walls were set as "CONCRETE", and the surfaces of the wall were assigned "INERT" for the FDS simulation. The properties of the concrete were set as follows: density (2100 kg/m^3), specific heat (879 J/(kg K)), and thermal conductivity were 1.10 W/(m K) according to Seike et al. (Seike et al., 2017).

In addition, to ensure that the numerical results are reliable and computationally correct, the time step was constrained such that the Courant-Friedrichs-Lewy (CFL) condition given in Eq. (3) was satisfied (Cheong et al., 2009; Gannouni and Maad, 2015):

$$\delta t \quad \max\left(\frac{u}{\delta x}, \frac{v}{\delta y}, \frac{w}{\delta z}\right) \leq 1 \tag{3}$$

The initial time step was specified automatically in FDS by dividing the grid size by the characteristic velocity of the flow. The value of the time step could be determined by Eq. (4):

$$\frac{5(\delta x \delta y \delta z)^{1/3}}{\sqrt{gH}} \tag{4}$$

For each time step during the calculations, the velocities u, v, and w were tested to ensure that the CFL condition was met. In a situation where CFL is greater than 1.0, the time step is set to 0.8 of its allowed peak value, and the velocities are recalculated and tested again. This is because the solutions to the equations cannot be updated with a time step greater than 1.0 which implies a parcel of fluid crossing the grid cell (Cheong et al., 2009). The time step was set between 0.8–1.0 for this study.

The fire was simulated utilizing a high-performance computer with FDS 6.7.6 using the large eddy simulation (LES) turbulence model. The whole domain was divided into four continuous domains and each domain was assigned to a processor to minimize the computational time. The ambient temperature for the simulation was set based on the measured value during the experiment., the set pressure was 101,325.0 Pa, and simulation time was set to 600.0 s

4. Temperature distribution

The temperature distribution in the underground environment is critical for the fire safety design and proactive measures such as the selection of appropriate tunnel lining materials, deployment of proper smoke control strategies, fire suppression systems, and emergency evacuation planning. To better enhance our understanding about the temperature evolution in mines, two main temperature indicators were considered for this investigation: temperature attenuation and maximum excess gas temperature beneath the tunnel ceiling.

Temperature attenuation may either be longitudinal or transverse (Li and Ingason, 2018). Longitudinal temperature attenuation indicates the temperature decay along the underground drift while the transverse temperature attenuation measures the temperature decay between the walls of the tunnel/drift. However, the longitudinal temperature variation along the mine airways is more important than the transverse temperature evolution as occupants tend to evacuate along the airways instead of moving zigzag between the walls of the mine airways. Thus, only the longitudinal temperature attenuation and maximum excess smoke temperature beneath the ceiling were considered for analysis in this study. A theoretical background of the two main temperature distribution indicators is presented below.

4.1. Longitudinal temperature attenuation

In an earlier study, an empirical model for temperature distribution beneath a tunnel ceiling was developed for fires that are centrally located in beamed channels as follow (Delichatsios, 1981):

$$\frac{\overline{\Delta T}}{\overline{\Delta T_0}}\left(\frac{l_b}{H}\right)^{1/3} = 0.49e^{\left\{-6.67tS_t\left(\frac{l_b}{H}\right)^{1/3}\right\}} \tag{5}$$

where $\overline{\Delta T_0}$ is the average temperature rise near the ceiling over the fire source, $\overline{\Delta T}$ is the average instantaneous temperature rise at a specified location from the fire axis, l_b represents the beam depth, H is the separation between the fire surface and the ceiling, and S_t is the Stanton number which was estimated to be 0.03 from the correlation of experimental data obtained from the study. The temperature attenuation conformed with exponential decay laws and subsequent investigations corroborated this finding. A later study by Hu et al. (Hu et al., 2013; Hu et al., 2008), involving series of full-scale tests in large tunnels and vehicular tunnels, showed that temperature beneath the ceiling in a longitudinally ventilated tunnel can be expressed as an exponential decay given by Eq. (6):

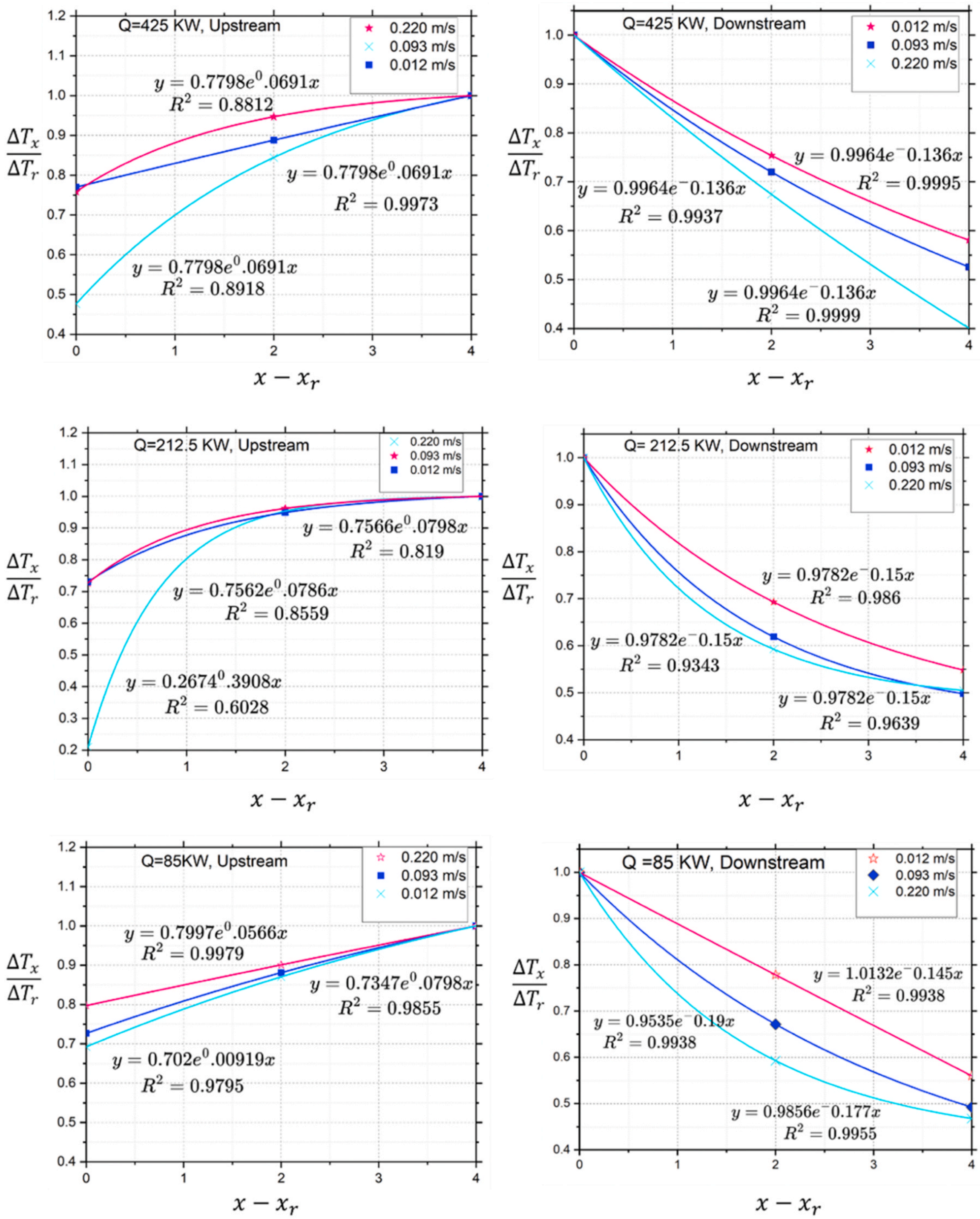

Fig. 10. Correlation of temperature attenuation in the mine drift for different fire sizes and longitudinal ventilation conditions.

$$\frac{\Delta T_x}{\Delta T_r} = e^{-\beta(x-x_r)} \tag{6}$$

where ΔT_x is the maximum increase in temperature x m away from a reference point, ΔT_r is the maximum increase in temperature at the reference point, x is the distance from the coordinate origin, x_r denotes the distance of separation between the fire and the coordinate origin, and β is the temperature attenuation factor.

Zhao et al. (Zhao et al., 2019) investigated the ceiling temperature distribution in a 1:20 reduced-scaled model tunnel and estimated the attenuation factor to be 0.536 for a tunnel fire with a two-point extraction ventilation system. Thus, using their attenuation factor, a modified Hu's equation was obtained as given by Eq. (7):

$$\frac{\Delta T_x}{\Delta T_r} = e^{-0.536(x-x_r)} \tag{7}$$

Another study involving a total of twelve tests in a model tunnel (with similarity of 1:23), Ingason and Li (Ingason and Li, 2010) demonstrated that the distribution of excess gas temperature beneath ceiling without ceiling mechanical smoke extraction can be expressed as a sum of two attenuation given by Eq. (8):

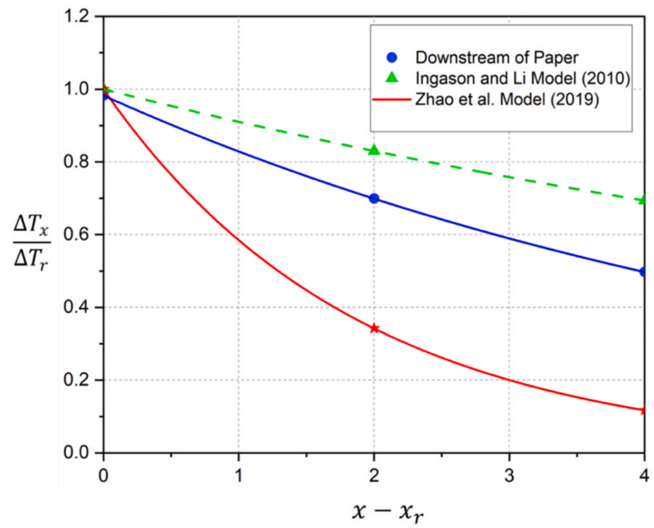

Fig. 11. Comparison of between temperature attenuation model developed and existing typical temperature attenuation models.

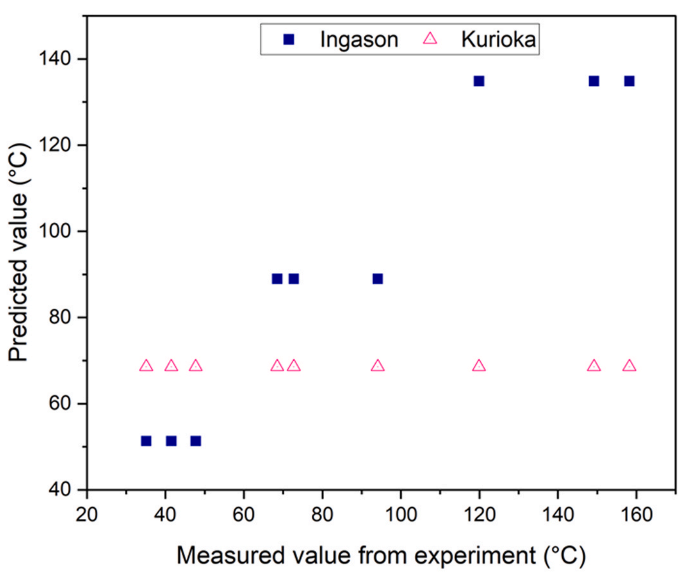

Fig. 12. Comparison of empirical models measured values of the smoke temperature rise beneath the ceiling.

$$\frac{\Delta T_x}{\Delta T_r} = 0.57e^{-0.13\left(\frac{x-x_r}{H}\right)} + 0.43e^{-0.048\left(\frac{x-x_r}{H}\right)} \tag{8}$$

Therefore, the generalized temperature decay model beneath tunnel/drift ceiling can be modified using exponential model as presented in Eq. (9):

$$\frac{\Delta T_x}{\Delta T_r} = Ae^{-F1\left(\frac{x-x_r}{H}\right)} + Be^{-F2\left(\frac{x-x_r}{H}\right)} \tag{9}$$

where *A, B, F1, and F2* are coefficients.

Although Hu's model with the assumption of zero entrainment of air from counter flow remains the most widely used model for tunnel ceiling temperature attenuation, most of the existing models were developed based on one-dimensional spreading phase (see Fig. 6) downstream of the fire (Zhao et al., 2018).

However, as seen from Fig. 6, it is also important to understand how the temperature evolves along the airway from a reference point upstream. This could help fire fighters and rescue teams to have an insight into the fire situation in the underground based on the observed temperature upstream of the fire. In this study, the temperature distribution upstream of the fire source was also examined and analyzed. Fig. 6 illustrates an emergency scenario where miners tried to escape from the fire and the fire-fighters/rescue team are advancing from the upstream position to put out the fire in other to evacuate the trapped occupants.

4.2. Maximum excess smoke temperature

The maximum temperature beneath the ceiling to which an underground structure or tunnel is exposed during a fire must be determined to identify the required fire protection needed for the tunnel structure (Han et al., 2021; Hu et al., 2013; Li and Ingason, 2012; Li et al., 2011; Tang et al., 2018; Zhang et al., 2021). The activation of fire suppression systems depends on the preset activation temperature, and the potential temperature rise expected during a fire outbreak (Li and Ingason, 2018; Tang et al., 2021; Yuan and Smith, 2015). To know the possible excess rise in temperature that may occur for these types of structures, several predictive models have been developed to foretell maximum temperature of thermal plume in an underground environment (Chen et al., 2020; Hu et al., 2013; Hu et al., 2006; Kurioka et al., 2003; Li and Ingason, 2012; Li et al., 2011).

(Kurioka et al., 2003) conducted an extensive experimental investigation into fire properties in the near field region and developed an empirical formula for the maximum temperature. Likewise, Li et al. (Li and Ingason, 2012; Li et al., 2011) applied the thermal plume theory to examine the maximum gas temperature beneath the tunnel ceiling and observed that the maximum gas temperature observed could be categorized into two regions for situations when the flame region is lower than the ceiling height. They showed that the relationship between the maximum gas temperature and the dimensionless heat release rate could be a linear or polynomial expression depending on the calculated values for the dimensionless ventilation velocity. Hu et al.'s group (Hu et al., 2013) studied the effect of tunnel slope on the maximum temperature of fire-induced hot gases and discovered that the gas temperature decay faster as the tunnel slope increases. Their investigation yielded a new empirical model that incorporated the effect of tunnel slope on temperature decay beneath tunnel ceiling.

In another study, the influence of tunnel sealing ratio on maximum temperature beneath ceiling was examined and a new empirical model was developed (Chen et al., 2020). The study introduced the concept of critical sealing ratio which was observed to decrease as the heat release rate increased.

Despite the numerous predictive models developed, many of these models could be derived by slight modifications from the Kurioka's (Kurioka et al., 2003) and Li's (Li et al., 2011) models. Thus, the two fundamental models were presented for further analysis in this study.

(Kurioka et al., 2003) model relates the maximum change in thermal plume temperature to a dimensionless HRR and Froude number as follows.

$$\frac{\Delta T_{\max}}{T_a} = \gamma\left(\frac{Q'^{2/3}}{Fr^{1/3}}\right)^{\varepsilon}, \tag{10}$$

where Q' is the dimensionless heat release rate of the fire expressed as: $Q' = \frac{Q}{(\rho_a C_p T_a g^{1/2} H_d^{5/2})}$,

Fr represents the Froude number and it is expressed as:

$Fr = \frac{U^2}{gH_d}$, where ρ_a, T_a, H_d, and u denote density, temperature of the ambient air, effective height of tunnel (that is, height from the surface of the fire source to the tunnel ceiling), and the longitudinal air velocity in the tunnel, respectively. The value of the constant parameters depends on the ratio of $\left(\frac{Q'^{2/3}}{Fr^{1/3}}\right)$ as follow:

$\left(\frac{Q'^{2/3}}{Fr^{1/3}}\right) < 1.35, \gamma = 1.77, \varepsilon = 6/5.$

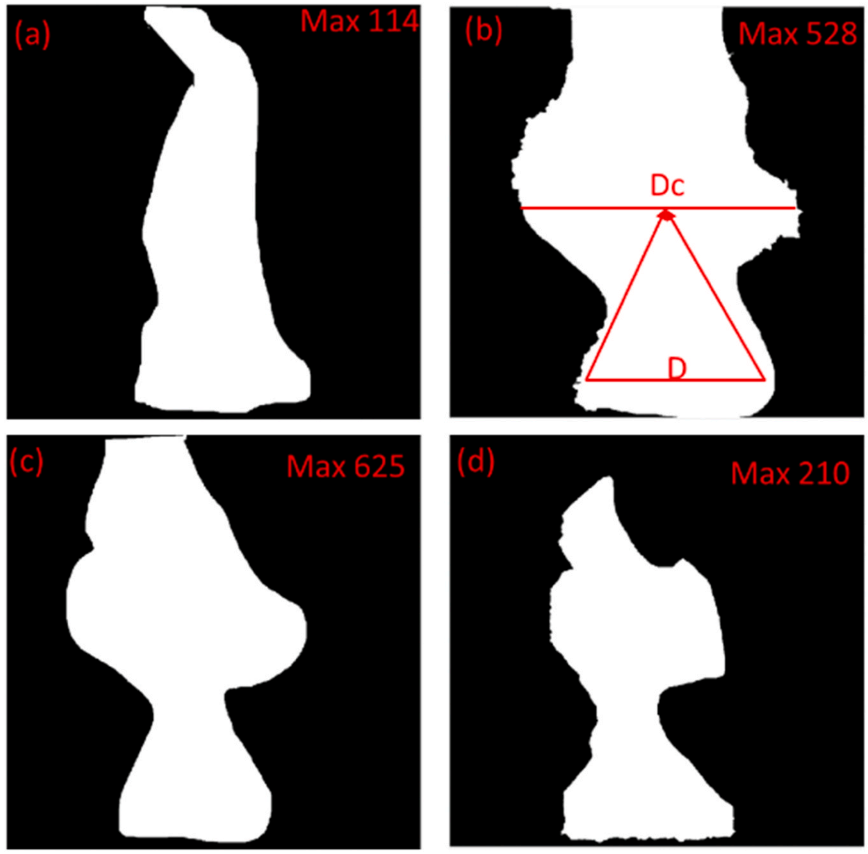

Fig. 13. Evolution of the flame shape for 212.5 KW fire.

Table 4
Comparison of empirical models for flame height calculations.

Reference	Formulae	Calculated (m)	Measured (m)	Error (%)
Thomas et al.,(Thomas, 1963)	$\frac{H}{D} = 42\left(\frac{m'}{\rho_a\sqrt{gD}}\right)^{0.61}$	3.7	2.4	-57%
Heskestad's model (Heskestad, 1995)	$\frac{H}{D} = \frac{0.235Q^{2/5}}{D} - 1.02$	2.9	2.4	-24%
Miao et al.'s (Miao et al., 2014)	$\frac{H}{D} = 1.73 + 0.33D^{-1.43}$	2.6	2.4	-9%

$\left(\frac{Q^{2/3}}{Fr^{1/3}}\right) \geq 1.35, \gamma = 2.54, \varepsilon = 0.$

Conversely, Li et al. (Li et al., 2011) expressed the maximum change in temperature rise as a function of the HRR and effective tunnel height based on the value of a dimensionless ventilation velocity as follows:

$$f(x) = \begin{cases} 17.5\frac{Q^{2/3}}{H_{ef}^{5/3}}, \& V' \leq 0.19 \\ \frac{Q}{Vb_{fo}^{1/3}H_{ef}^{5/3}}, \& V' > 0.19 \end{cases} \quad (11)$$

where Q, H_{ef}, V, V', and b_{fo}, represent the heat release rate, effective tunnel height, ventilation velocity, dimensionless ventilation velocity, and radius of the fire pool, respectively. The dimensionless ventilation velocity is given by:

$$V' = \frac{V}{\left(\frac{gQ}{b_{fo}\rho_a c_p T_a}\right)^{1/3}}.$$

5. Results and discussion

5.1. Air flow/ Longitudinal ventilation velocity

The results of the longitudinal velocity obtained from the point traverse anemometer reading are presented in Table 2. The calculated airflow at the fan exhaust was 0.24 m^3/s, 2.97 m^3/s, and 5.42 m^3/s for ventilation conditions of 0%, 50%, and 100%, respectively. The corresponding longitudinal ventilation velocity obtained was 0.220 m/s, 0.093 m/s, and 0.012 m/s for 100 % and 50 % smoke extraction rate, and natural ventilation conditions, respectively. From Table 2, virtually all the transverse points recorded "0.00″ for Exp 3, Exp 4, and Exp 5. This implies that there is no airflow along the traverse point. This is because the fan was put off for those experiments. As shown in Table 1, the ventilation rate is 0% for these experiments.

5.2. Heat release rate (HRR) calculations

The HRR results in the order of decreasing maximum temperature are presented in Table 3. Based on Table 3, the fire size had a profound effect on the burning rate while longitudinal ventilation had a negligible effect on the burning rate due to the very low ventilation velocity observed in the mine during the fire tests. For instance, considering test experimental cases 5 and 6, a decrease of fire size to about a half may cause the burning time to increase with a factor of up to 4.5 if the ventilation is kept constant.

5.3. Temperature attenuation factor

A typical temperature evolution curves observed during the test is shown in Fig. 7. The case presented was for Test No 2 (i.e., 0.7 D, 50% Vent). This pattern was the same for all other test cases. The details of

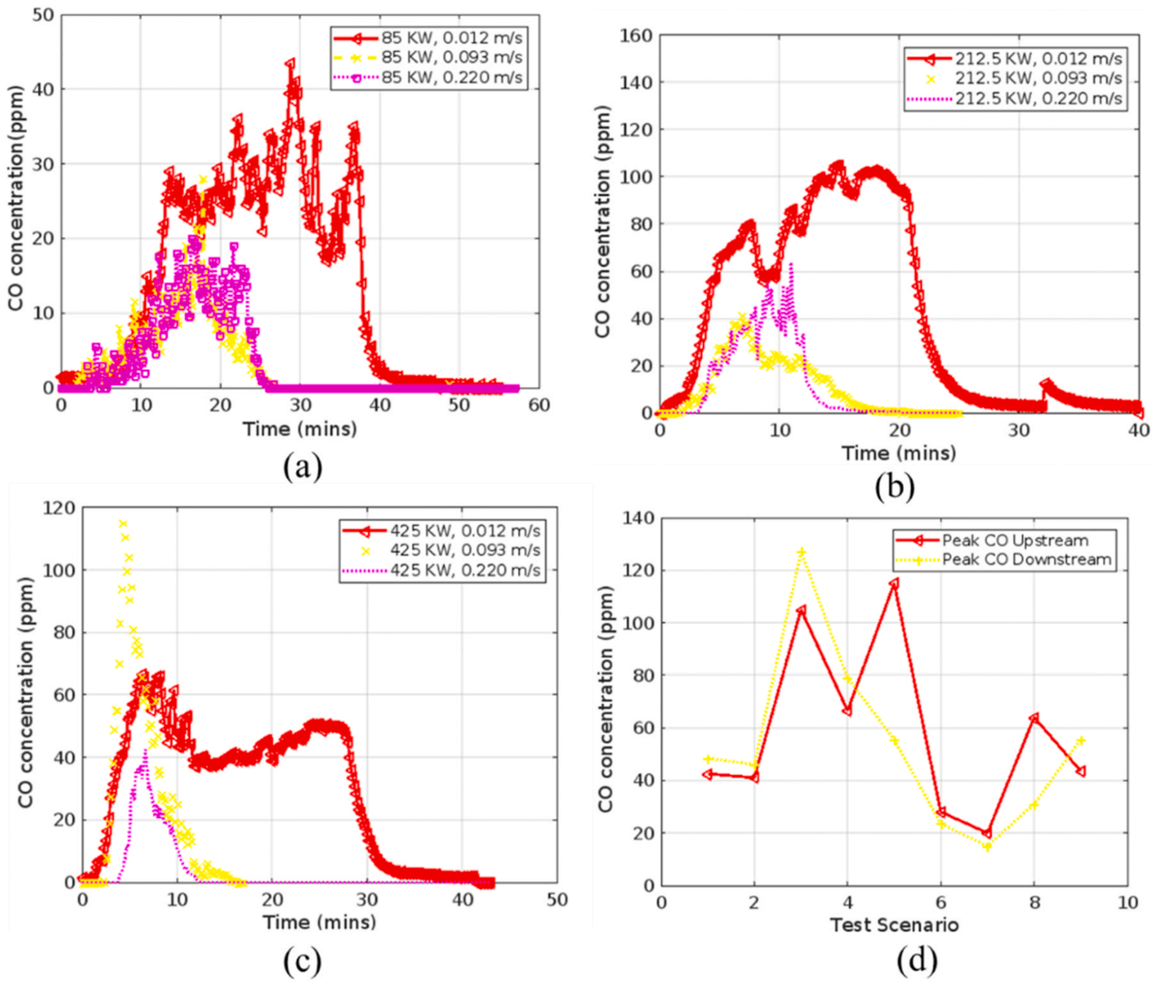

Fig. 14. Typical CO evolution curve and comparison of peak CO concentration for upstream and downstream positions.

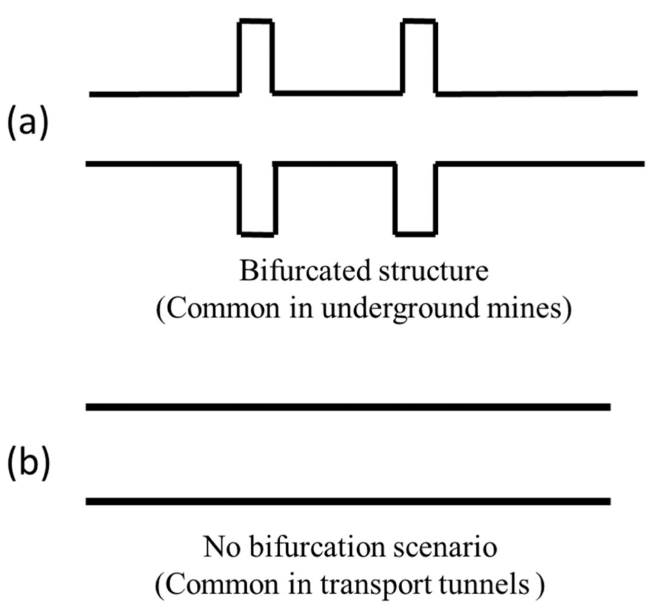

Fig. 15. Schematic of bifurcated and non-bifurcated underground space.

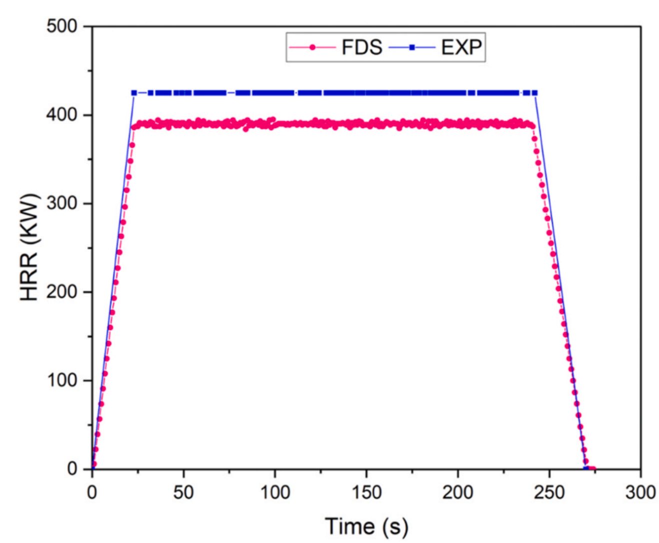

Fig. 16. Comparison of the HRR curve for the experiment and simulation.

temperature evolution for other cases are not presented since our primary focus was the maximum smoke temperature at each measuring station. Hence, for the purpose of this analysis, only the maximum smoke temperature was considered.

The results of the observed maximum smoke temperature are presented in Fig. 8 and Fig. 9. Fig. 8 shows the temperature distribution at the mine ceiling, while Fig. 9 shows that temperature evolution 1 m below the mine roof. The negative x-axis represents upstream locations,

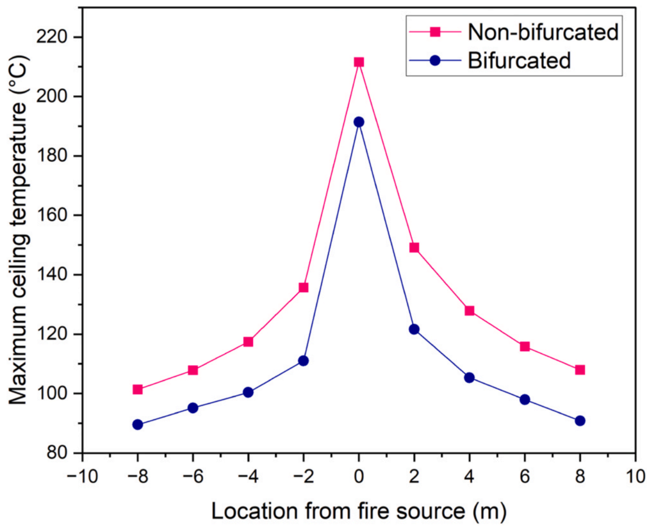

Fig. 17. Comparison of the maximum excess smoke temperature for the bifurcated and non-bifurcated scenario.

and the positive distance signs represent downstream positions of fire. Generally, the maximum temperature is observed to decrease as the distance from the fire source is increases.

The maximum rise in smoke temperature beneath the mine roof (presented in Fig. 8) within the quasi-steady stage at the different measuring stations were employed for subsequent calculations of temperature decay. The analysis of temperature decay in Fig. 10 showed the overall temperature attenuation was greater in the downstream (attenuation factor of 0.17) than in the upstream (attenuation factor of 0.12). This may be due to smoke roll-back in the upstream. Also, this could be due the smoke mixing with fresh air faster as the smoke travel downstream towards the ventilation exhaust.

For the derivation of the attenuation models of both upstream and downstream of the fire, an improved technique (Tao and Zeng, 2022), which incorporating a two-dimensional spreading phase for the temperature distribution was introduced instead of the conventional one-dimensional temperature decay model. Firstly, the smoke temperature, T_x was normalized measured by the thermocouples from a distance x from the fire to a dimensionless temperature $\Delta T_{ND,x}$ by a reference value T_r and the ambient air temperature T_a as follow:

$$\Delta T_{ND,x} = \frac{T_x - T_a}{T_r - T_a}. \tag{12}$$

The reference temperatures T_r for the upstream and downstream positions were taken at stations S3 and station S5 (as shown in Figs. 4), 2 (m) upstream and downstream of the fire source, respectively. The dimensionless normalized temperatures were plotted against the distance of separation of the thermocouples measuring stations to the fire source as seen in Fig. 10. The experimental data from each test was fitted to an exponential function using the following equations:

$$\Delta T_{ND,x} = a.e^{b(x-x_r)}. \tag{13}$$

The dimensionless normalized temperatures can be properly fitted using the exponential function (Zhao et al., 2019). The average value of the attenuation factors was determined and used for developing the empirical model in this study. Finally, a two-dimensional spreading phase empirical model that could predict the temperature distribution for an axisymmetric fire in a mine drift was developed. Based on the results in Fig. 10, the semi-empirical calculation model is summarized as follows:

$$f(x) = \begin{cases} 0.98e^{-0.12(x-x_r)} & upstream \quad of \quad fire \quad source \\ 0.98e^{-0.17(x-x_r)} & downstream \quad of \quad fire \quad source \end{cases} \tag{14}$$

A comparison of the new predictive model with existing models was done to validate our new model. Ingason and Li's model (Ingason and Li, 2010) developed a model using a reduced-scale tunnel with no mechanical smoke extraction. Zhao et al.'s model (Zhao et al., 2019) also developed a temperature attenuation model using a reduced scale model tunnel but with a two point mechanical smoke extraction point. However, the attenuation model developed in this study was based on a single-point smoke extraction system. As deduced from Fig. 11, that the temperature decay rate increased as more smoke extraction point was added compared to the case with no mechanical smoke extraction.

5.4. Maximum excess smoke temperature

Similarly, the maximum smoke temperature during the experiment was measured and compared to two commonly used empirical models for predicting the maximum temperature rise beneath the tunnel ceiling as analyzed in Section 4.2. The results are presented in Fig. 12. The predicted maximum smoke temperature rise was plotted against the measured values. It was observed that Li et al.'s model demonstrated better predictive capability compared to the Kurioka's et al. model. Kurioka et al.'s model predicted a constant smoke temperature for the nine experimental cases which implies that the accuracy of Kurioka et al.'s model may be greatly affected for large values of $\left(\frac{Q^{2/3}}{Fr^{1/3}}\right)$ since $\left(\frac{Q^{2/3}}{Fr^{1/3}}\right)$ was found to be greater than 1.35 for all the experimental cases

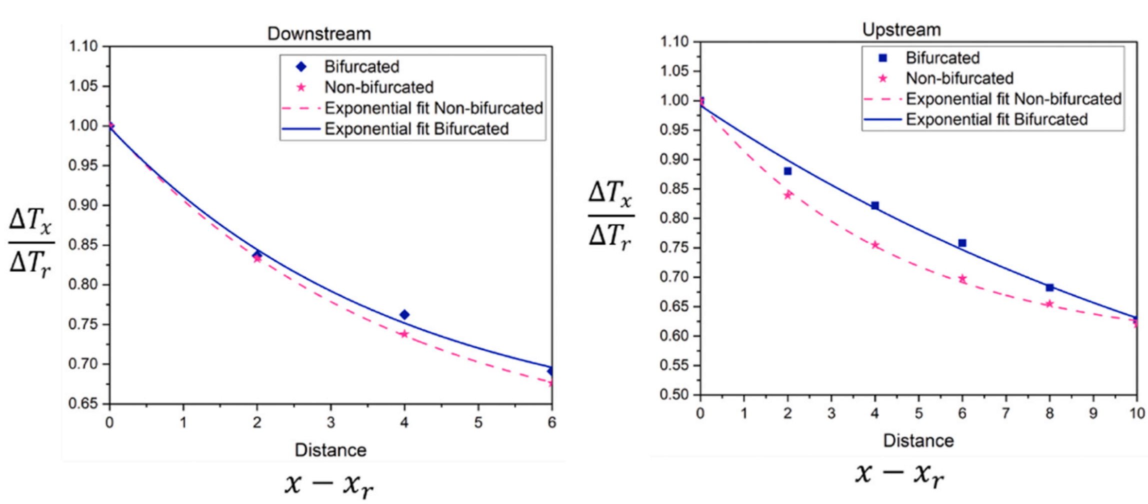

Fig. 18. Comparison of temperature attenuation for bifurcated and non-bifurcated scenarios.

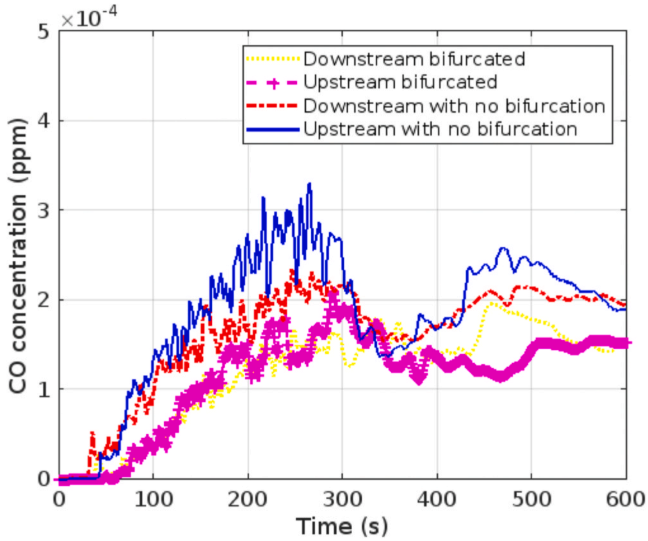

Fig. 19. Comparison of the CO concentration for bifurcated and non-bifurcated scenarios.

considered in this investigation. This finding corroborates previous study by confirming that a value of $\left(\frac{Q^{2/3}}{Fr^{1/3}}\right) > 1.35$ leads to a constant $\Delta T_{\max}/T_a$regardless of the HRR (Ji et al., 2012).

Analysis of the Kurioka et al.'s model indicates that the maximum gas temperature becomes infinitely large when the ventilation velocity tends to zero (Ji et al., 2012; Li and Ingason, 2012; Li et al., 2011). This implies that the model cannot predict the maximum temperature accurately for low ventilation velocity. The results from this study showed that Li et al.'s model has a better performance in predicting the maximum gas temperature for a very small ventilation velocity which further validate the results from the study by Li and Ingason (Li and Ingason, 2012). Therefore, for a low ventilation velocity ($i.eV' \leq 0.19$), the maximum temperature beneath ceiling in a mine drift was mainly influenced by the HRR. Thus, for a longitudinal ventilation velocity, V', ≤ 0.19, the maximum excess temperature in a mine drift could be determined by Eq. (15):

$$T_{\max} = \begin{cases} 17.5\dfrac{Q^{2/3}}{H_{ef}^{5/3}} \\ Constant \end{cases} \tag{15}$$

5.5. Thermal image and flame analysis

Fig. 13 shows the flame evolution for a 212.5KW fire. Fig. 13 (a), (b), (c), and (d) depict the flame shape for the fire growth stage, flashover stage, burning stage, and decay stage, respectively. D denotes the pool fire diameter while D_c is the diameter of the flame. This is a typical evolution for the different fire sizes. Fig. 13 displays that D_c becomes greater than D once the fire reaches the flashover stage and the value starts to decrease through the decay stage to the complete burnout.

The flame height was measured for the different burning stages and the maximum flame height was recorded. The maximum flame height observed was 1.2 m for a pool fire with diameter of 0.5 m. This corresponds to $H/D = 2.4$. The comparison of the observed experimental data with some exiting empirical model is presented in Table 4. By computing the error from the different empirical models, Miao et al.'s model (Miao et al., 2014), which represents the simplest approach for computing the flame height, based on the diameter of the pool gives the closest approximation of H/D. Heskestad's model (Heskestad, 1995) computed a value within an ±30%. However, Thomas' model (Thomas, 1963) over predicted H/D for this scenario. One reason that may account for this discrepancy may be due to the level of details required to accurately compute the value of H/D using Thomas' formulae.

5.6. CO evolution in the tunnel

The CO profile for each of the test cases upstream of the fire is presented in Fig. 14 (a) to (c). Generally, the CO concentration is observed to be greatly influenced by ventilation conditions. From Fig. 14 (a) & (b), it can be observed that increasing the ventilation rate from 0% to 100% reduced the maximum CO by up to about 40%. Even though a slight deviation is seen in Fig. 14 (c), the spike in CO level when the ventilation rate was 50% could probably be attributed to an instrumental error. Analysis of the peak CO concentration upstream and downstream of the fire presented in Fig. 14 (b) shows some competing trends.

For tests 1 to 4 and test 9, the peak CO concentration was found to be higher downstream than in the upstream. However, this trend can be seen to take a swing for tests 5 to 8, where the peak CO concentration upstream was higher than the measured value downstream of the mine. Additionally, the inconsistency in the CO concentration trend may result from the leakages in the tunnel because of the presence of multiple bifurcation in the underground test area. The prior study by Yuan et al. (Yuan et al., 2016) illustrated that airflow leakages could cause a reduction in the concentration of CO in an underground entries.

5.7. Influence of bifurcation

Prior to conducting the FDS simulation to investigate the influence of bifurcation, the HRR of the experimental and simulation was compared to check for consistency. The results of the HRR histories for both FDS and experiment are presented in Fig. 15. The peak HRR measured during the experiment was 425.0 KW while that obtained from the simulation approximately 400.0 KW which was acceptable because the deviation was only about 5.9%. In addition, the primary objective of the simulation was not to evaluate FDS accuracy but to extend FDS capability to investigate how bifurcations present in real underground mines may influence the maximum smoke gas temperature compared to tunnel fires . A schematic of the dichotomy between bifurcated and non-bifurcated scenario is shown in Fig. 15. The first scenario showing bifurcation in Fig. 15 (a) is common in mines because of the several development faces that may be present in the mines while the second scenario represents the ubiquitous cases mostly found in road tunnels. For this study, the no-bifurcation condition was developed by simply blocking off the rooms within the room-and-pillar mine with a concrete obstruction in the FDS model.

Maximum smoke temperature measured upstream and downstream for the bifurcated and non-bifurcated scenario from the FDS simulation is presented in Fig. 17. Based on Fig. 17, the maximum ceiling jet temperature increased when there was no bifurcation in the drift. However, the temperature evolution for both scenarios followed a similar trend. For both bifurcated and non-bifurcated scenarios, the ceiling jet temperature decreased as we moved away from the fire source both in the upstream and downstream directions.

Additionally, it can be observed the curve of the exponential fitting does not completely overlap for the bifurcated and non-bifurcated scenarios which indicates that the rate of temperature decay for the two cases differ, as depicted in Fig. 18. Based on the results in Fig. 18, the empirical model for the bifurcated and non-bifurcated scenario can be summarized as follow:

$$f(x) = \begin{cases} 0.9807e^{-0.052(x-x_r)}, Bifurcated \\ 0.9510e^{-0.056(x-x_r)}, Non-bifurcated \end{cases} \tag{16}$$

Likewise, the spread of toxic carbon monoxide was examined to investigate how bifurcation affects the toxicity concentration. This is the main cause of fatality in the underground mine fires. Two gas detectors placed 2.0 m upstream and downstream of the fire in the FDS model was used to measure the CO concentration during the simulation. The result of the CO concentration is presented in Fig. 19. The findings indicates that tunnel bifurcation had a strong influence on the CO concentration in the underground space. As can be seen in the upstream and downstream positions, the CO concentration was higher for non-bifurcated cases, which indicates that bifurcation could serve as a cross-passage for toxic gases to diffuse quicker to other portions of the confined space thus reducing the overall peak value of the toxic gas concentration.

6. Conclusions

Full-scale fire tests were conducted in an underground mine drift and the analysis of temperature attenuation and the maximum excess gas temperature beneath a mine drift was presented in this study using experimental and theoretical approach. A CFD model was developed and validated using the experimental data and the model was extended to study the influence of bifurcation on the temperature and toxic gases spread in an underground mine drift. The temperature evolution upstream and downstream of the mine drift were fitted using an exponential correlation and a new empirical model of temperature attenuation given by Eq. (14) was proposed. The attenuation model upstream of fire could predict the temperature rise as we moved towards the fire from any upstream location. This correlation is valid for HRR value between 85–425 KW and maximum excess gas temperature of up to 160 °C. This type of prognosticative attenuation model will further improve firefighting and suppression strategy as responders move towards the fire zone during an emergency.

Temperature attenuation, maximum excess gas temperature, and CO evolution were observed to be strongly influenced by ventilation conditions. Furthermore, experimental data were used to verify the existing formulae for the maximum excess gas temperature beneath a tunnel/mine drift. Tests results showed a good agreement with Li et al.'s model compared to Kurioka et al.'s model. Also, the fire pool diameter was observed to be sufficient for determining flame height characteristics based on Miao's empirical model. Test results showed a good correlation between the measured flame height for the experimental and calculated values . The influence of different fire locations, such as fires in the blind heading and effective tunnel height (i.e., the separation between the bottom of the fire source and the tunnel ceiling) was not considered in this paper, therefore, it may influence the temperature and smoke propagation and will be investigated in future research.

Furthermore, bifurcation showed a strong influence on the temperature evolution and product of combustion spread in underground environments. The magnitude of the influence of bifurcation parameters was not considered in this study and would be investigated in future work. Additionally, there are several combustible materials that could lead to fires in the underground mines. These materials include wood, coal, rubber, belt, equipment etc. Future studies should evaluate the combustibility of these materials as only diesel pool combustion was investigated in this study. Finally, the findings from this study could serve as the fire field data in building and optimizing emergency evacuation plans, in addition to validating existing CFD models for underground mines and other confined space environments.

Declaration of Competing Interest

The authors declare the following financial interests/personal relationships which may be considered as potential competing interests: Guang Xu reports financial support was provided by National Institute for Occupational Safety and Health (NIOSH).

Acknowledgements

This research is funded by the National Institute for Occupational Safety and Health (NIOSH) under contract number 75D30120CO8913 and 1 U60OH012350-01-00. The findings and conclusions in this report are those of the authors and do not represent the official position of the National Institute for Occupational Safety and Health, Centers for Disease Control and Prevention; nor does mention of trade names, commercial practices, or organizations imply endorsement by the U.S. Government.

References

Bahrami, D., Zhou, L., Yuan, L., 2021. Field verification of an improved mine fire location model. Min., Metall. Explor. 38 (1), 559–566. https://doi.org/10.1007/s42461-020-00314-6.

Chang, P., Xu, G., Zhou, F., Mullins, B., Abishek, S., 2019. Comparison of underground mine DPM simulation using discrete phase and continuous phase models. Process Saf. Environ. Prot. 127, 45–55. https://doi.org/10.1016/j.psep.2019.04.027.

Chen, C., Zhang, Y., Lei, P., Jiao, W., 2020. A study for predicting the maximum gas temperature beneath ceiling in sealing tactics against tunnel fire. Tunn. Undergr. Space Technol. 98, 103275 https://doi.org/10.1016/j.tust.2019.103275.

Chen, Z., Liu, Z., Huang, L., Niu, G., Yan, J., Wang, J., 2023. Research on the effect of ceiling centralized smoke exhaust system with air curtains on heat confinement and plug-holing phenomenon in tunnel fires. Process Saf. Environ. Prot. 169, 646–659. https://doi.org/10.1016/j.psep.2022.11.054.

Cheong, M., Spearpoint, M., Fleischmann, C., 2009. Calibrating an FDS simulation of goods-vehicle fire growth in a tunnel using the runehamar experiment. J. fire Prot. Eng. 19 (3), 177–196.

Delichatsios, M.A., 1981. The flow of fire gases under a beamed ceiling. Combust. flame 43, 1–10.

Dong, S., Lu, X., Wang, D., Wang, H., Zheng, K., Shi, Q., Chen, M., 2017. Experimental investigation of the fire-fighting characteristics of aqueous foam in underground goaf. Process Saf. Environ. Prot. 106, 239–245. https://doi.org/10.1016/j.psep.2016.12.009.

Düzgün, H.S., Leveson, N., 2018. Analysis of soma mine disaster using causal analysis based on systems theory (CAST). Saf. Sci. 110, 37–57. https://doi.org/10.1016/j.ssci.2018.07.028.

Fernández-Alaiz, F., Castañón, A.M., Gómez-Fernández, F., Bascompta, M., 2020. Mine fire behavior under different ventilation conditions: Real-scale tests and CFD modeling. Appl. Sci. 10 (10), 3380.

Fernández-Alaiz, F., Castañón, A.M., Gómez-Fernández, F., Bernardo-Sánchez, A., Bascompta, M., 2020. Determination and fire analysis of gob characteristics using CFD. Energies 13 (20), 5274.

Fernánez-Alaiz, F., Castañón, A.M., Gómez-Fernández, F., Bernardo-Sánchez, A., Bascompta, M., 2020. Analysis of the fire propagation in a sublevel coal mine. Energies 13 (14), 3754.

Gannouni, S., Maad, R.B., 2015. Numerical study of the effect of blockage on critical velocity and backlayering length in longitudinally ventilated tunnel fires. Tunn. Undergr. Space Technol. 48, 147–155. https://doi.org/10.1016/j.tust.2015.03.003.

Gehandler, J., 2015. Road tunnel fire safety and risk: a review. Fire Sci. Rev. 4 (1), 2 https://doi.org/10.1186/s40038-015-0006-6.

Haghighat, A., Luxbacher, K., Lattimer, B.Y., 2018. Development of a methodology for interface boundary selection in the multiscale road tunnel fire simulations. Fire Technol. 54 (4), 1029–1066. https://doi.org/10.1007/s10694-018-0724-0.

Han, J., Wang, Z., Geng, P., Wang, F., Wen, J., Liu, F., 2021. The effect of blockage and tunnel slope on smoke spread and ceiling temperature distribution in a natural-ventilated metro depot. Energy Build. 253, 111540 https://doi.org/10.1016/j.enbuild.2021.111540.

Hansen, R., 2019. Design of fire scenarios for Australian underground hard rock mines–applying data from full-scale fire experiments. J. Sustain. Min. 18 (4), 163–173.

Hansen, R.,Ingason, H.2013b, *Full-scale fire experiments with mining vehicles in an underground mine*.

Hansen, R., Ingason, H. , 2013a. *Full-scale fire experiments with mining vehicles in an underground mine* (978-91-7485-115-1 (ISBN)). (Studies in Sustainable Technology / Forskningsrapport, Issue. http://urn.kb.se/resolve?urn=urn:nbn:se:mdh:diva-20912.

Hansen, R., Ingason, H., 2013c. Heat release rate measurements of burning mining vehicles in an underground mine. Fire Saf. J. 61, 12–25. https://doi.org/10.1016/j.firesaf.2013.08.009.

Heskestad, G. , 1995. Fire plumes, SFPE handbook of fire protection engineering. *Nation Fire Protection Association, Quincy, Massachusetts*.

Hong, Y., Kang, J., Fu, C., 2022. Rapid prediction of mine tunnel fire smoke movement with machine learning and supercomputing techniques. Fire Saf. J. 127, 103492 https://doi.org/10.1016/j.firesaf.2021.103492.

Hu, L., Chen, L., Wu, L., Li, Y., Zhang, J., Meng, N., 2013. An experimental investigation and correlation on buoyant gas temperature below ceiling in a slopping tunnel fire. Appl. Therm. Eng. 51 (1-2), 246–254.

Hu, L.H., Huo, R., Peng, W., Chow, W.K., Yang, R.X., 2006. On the maximum smoke temperature under the ceiling in tunnel fires. Tunn. Undergr. Space Technol. 21 (6), 650–655. https://doi.org/10.1016/j.tust.2005.10.003.

Hu, L.H., Zhou, J.W., Huo, R., Peng, W., Wang, H.B., 2008. Confinement of fire-induced smoke and carbon monoxide transportation by air curtain in channels. J. Hazard. Mater. 156 (1), 327–334. https://doi.org/10.1016/j.jhazmat.2007.12.041.

Huang, P., Chen, M., Chen, K., Zhang, H., Yu, L., Liu, C., 2022. A combined real-time intelligent fire detection and forecasting approach through cameras based on

computer vision method. Process Saf. Environ. Prot. 164, 629–638. https://doi.org/10.1016/j.psep.2022.06.037.
Huang, Y., Li, Y., Dong, B., Li, J., Liang, Q., 2018. Numerical investigation on the maximum ceiling temperature and longitudinal decay in a sealing tunnel fire. Tunn. Undergr. Space Technol. 72, 120–130.
Ingason, H., Li, Y.Z., 2010. Model scale tunnel fire tests with longitudinal ventilation. Fire Saf. J. 45 (6-8), 371–384.
Iqbal, A., Xu, G., Pushparaj, R.I., Salami, O.B., 2023. Analysis of small-scale lithium-ion batteries under thermal abuse. Underground Ventilation. CRC Press,, pp. 578–586.
Ji, J., Fan, C., Zhong, W., Shen, X., Sun, J., 2012. Experimental investigation on influence of different transverse fire locations on maximum smoke temperature under the tunnel ceiling. Int. J. Heat. Mass Transf. 55 (17-18), 4817–4826.
Kamran, M., Wattimena, R.K., Armaghani, D.J., Asteris, P.G., Jiskani, I.M., Mohamad, E. T., 2023. Intelligent based decision-making strategy to predict fire intensity in subsurface engineering environments. Process Saf. Environ. Prot. 171, 374–384. https://doi.org/10.1016/j.psep.2022.12.096.
Khan, F.I., Abbasi, S.A., 1999. Major accidents in process industries and an analysis of causes and consequences. J. Loss Prev. Process Ind. 12 (5), 361–378. https://doi.org/10.1016/S0950-4230(98)00062-X.
Kirytopoulos, K., Konstandinidou, M., Nivolianitou, Z., Kazaras, K., 2014. Embedding the human factor in road tunnel risk analysis. Process Saf. Environ. Prot. 92 (4), 329–337. https://doi.org/10.1016/j.psep.2014.03.006.
Kurioka, H., Oka, Y., Satoh, H., Sugawa, O., 2003. Fire properties in near field of square fire source with longitudinal ventilation in tunnels. Fire Saf. J. 38 (4), 319–340.
Lee, Y.S., Ghazali, F.E.M., 2018. Major functional risks for operation and maintenance of tunnelling projects. ESTEEM 14.
Lei, B., He, B., Zhao, Z., Xu, G., Wu, B., 2021. A method for identifying the fire status through ventilation systems using tracer gas for improved rescue effectiveness in roadway drivage of coal mines. Process Saf. Environ. Prot. 151, 151–157. https://doi.org/10.1016/j.psep.2021.05.010.
Li, Y.Z., Ingason, H., 2012. The maximum ceiling gas temperature in a large tunnel fire. Fire Saf. J. 48, 38–48.
Li, Y.Z., Ingason, H., 2018. Overview of research on fire safety in underground road and railway tunnels. Tunn. Undergr. Space Technol. 81, 568–589.
Li, Y.Z., Lei, B., Ingason, H., 2011. The maximum temperature of buoyancy-driven smoke flow beneath the ceiling in tunnel fires. Fire Saf. J. 46 (4), 204–210.
Liu, C., Zhong, M., Shi, C., Zhang, P., Tian, X., 2017. Temperature profile of fire-induced smoke in node area of a full-scale mine shaft tunnel under natural ventilation. Appl. Therm. Eng. 110, 382–389. https://doi.org/10.1016/j.applthermaleng.2016.08.147.
Lu, X., Weng, M., Liu, F., Wang, F., Han, J., Cheung, S.C., 2022. Study on smoke temperature profile in bifurcated tunnel fires with various bifurcation angles under natural ventilation. J. Wind Eng. Ind. Aerodyn. 225, 105001 https://doi.org/10.1016/j.jweia.2022.105001.
Mavhura, E., 2019. A systems approach for assessing emergency preparedness in underground mines of Zimbabwe. Resour. Policy 62, 1–8. https://doi.org/10.1016/j.resourpol.2019.03.005.
McGrattan, K., Hostikka, S., McDermott, R., Floyd, J., Weinschenk, C., Overholt, K., 2013. Fire dynamics simulator technical reference guide volume 1: mathematical model. NIST Spec. Publ. 1018 (1), 175.
McGrattan, K., Peacock, R., Overholt, K., 2016. Validation of fire models applied to nuclear power plant safety. Fire Technol. 52, 5–24.
McGrattan, K.B., Peacock, R.D., Overholt, K.J. , 2014. *Verification and validation of selected fire models for nuclear power plant applications supplement 1*. U. S. N. R. C. NUREG-1824. https://www.nist.gov/publications/verification-and-validation-selected-fire-models-nuclear-power-plant-applications-1.
Miao, Z., Wenhua, S., Ji, W., Zhen, C., 2014. Accident consequence simulation analysis of pool fire in fire dike. Procedia Eng. 84, 565–577.
Ntzeremes, P., Kirytopoulos, K., 2019. Evaluating the role of risk assessment for road tunnel fire safety: a comparative review within the EU. J. Traffic Transp. Eng. (Engl. Ed.) 6 (3), 282–296.
Oka, Y., Atkinson, G.T., 1995. Control of smoke flow in tunnel fires. Fire Saf. J. 25 (4), 305–322. https://doi.org/10.1016/0379-7112(96)00007-0.
Overholt, K.J. , 2014. *Verification and validation of commonly used empirical correlations for fire scenarios*. US Department of Commerce, National Institute of Standards and Technology.
Salami, O., Xu, G. , 2022. EXPERIMENTAL INVESTIGATION OF FIRE AND PRODUCT OF COMBUSTION (POC) SPREAD IN UNDERGROUND MINES: A CASE STUDY. SME Annual Conference and Expo 2022,
Salami, O.B., Xu, G., Kumar, A.R., Pushparaj, R.I., Iqbal, A., 2023b. Fire-induced temperature attenuation under the influence of a single ceiling smoke extraction point in a bifurcated drift. Underground Ventilation. CRC Press, pp. 399–410.
Salami, O.B., Xu, G., Kumar, A.R., Pushparaj, R.I., 2023a. Underground mining fire hazards and the optimization of emergency evacuation strategies (EES): The issues, existing methodology and limitations, and way forward. Process Saf. Environ. Prot. 177, 617–634. https://doi.org/10.1016/j.psep.2023.07.012.
Seike, M., Kawabata, N., Hasegawa, M., 2017. Quantitative assessment method for road tunnel fire safety: development of an evacuation simulation method using CFD-derived smoke behavior. Saf. Sci. 94, 116–127. https://doi.org/10.1016/j.ssci.2017.01.005.
Tang, F., Cao, Z., Palacios, A., Wang, Q., 2018. A study on the maximum temperature of ceiling jet induced by rectangular-source fires in a tunnel using ceiling smoke extraction. Int. J. Therm. Sci. 127, 329–334. https://doi.org/10.1016/j.ijthermalsci.2018.02.001.
Tang, W., Yuan, L., Bahrami, D., Rowland, J., 2021. Water spray suppression of leaked oil fires: a numerical study. Mine Ventilation. CRC Press,, pp. 309–316.
Tao, L., Zeng, Y., 2022. Effect of single-side centralized exhaust on smoke control and temperature distribution in longitudinal ventilation tunnel fires. Tunn. Undergr. Space Technol. 119, 104241.
Thomas, P., 1963. The size of flames from natural fires. Symp. . (Int.) Combust.
Wang, Y., Si, G., Xiang, Z., Oh, J., Belle, B., Webb, D., 2022. A theoretical goaf resistance model based on gas production analysis in goaf gas drainage. Int. J. Coal Geol. 264, 104140.
Weng, M.-c, Lu, X.-l, Liu, F., Shi, X.-p, Yu, L.-x, 2015. Prediction of backlayering length and critical velocity in metro tunnel fires. Tunn. Undergr. Space Technol. 47, 64–72. https://doi.org/10.1016/j.tust.2014.12.010.
Xiang, Z., Si, G., Wang, Y., Belle, B., Webb, D., 2021. Goaf gas drainage and its impact on coal oxidation behaviour: a conceptual model. Int. J. Coal Geol. 248, 103878.
Xu, G., Jong, E.C., Luxbacher, K.D., McNair, H.M., 2016. Effective utilization of tracer gas in characterization of underground mine ventilation networks. Process Saf. Environ. Prot. 99, 1–10. https://doi.org/10.1016/j.psep.2015.10.001.
Yuan, L., Smith, A.C., 2015. Numerical modeling of water spray suppression of conveyor belt fires in a large-scale tunnel. Process Saf. Environ. Prot. 95, 93–101. https://doi.org/10.1016/j.psep.2015.02.018.
Yuan, L., Zhou, L., Smith, A.C., 2016. Modeling carbon monoxide spread in underground mine fires. Appl. Therm. Eng. 100, 1319–1326. https://doi.org/10.1016/j.applthermaleng.2016.03.007.
Yuan, L., Thomas, R.A., Rowland, J.H., Zhou, L., 2018. Early fire detection for underground diesel fuel storage areas. Process Saf. Environ. Prot. 119, 69–74. https://doi.org/10.1016/j.psep.2018.07.022.
Zhang, X., Lin, Y., Shi, C., Zhang, J., 2021. Numerical simulation on the maximum temperature and smoke back-layering length in a tilted tunnel under natural ventilation. Tunn. Undergr. Space Technol. 107, 103661.
Zhao, P., Yuan, Z., Yuan, Y., Yu, N., Yu, T., 2019. A study on ceiling temperature distribution and critical exhaust volumetric flow rate in a long-distance subway tunnel fire with a two-point extraction ventilation system. Energies 12 (8), 1411.
Zhao, S., Liu, F., Wang, F., Weng, M., 2018. Experimental studies on fire-induced temperature distribution below ceiling in a longitudinal ventilated metro tunnel. Tunn. Undergr. Space Technol. 72, 281–293.
Zhou, L., 2009. Improvement of the mine fire simulation program MFIRE.
Zhou, L., Yuan, L., Bahrami, D., Thomas, R.A., Rowland, J.H., 2018. Numerical and experimental investigation of carbon monoxide spread in underground mine fires. J. fire Sci. 36 (5), 406–418.
Zhu, H., Shen, Y., Yan, Z., Guo, Q., Guo, Q., 2016. A numerical study on the feasibility and efficiency of point smoke extraction strategies in large cross-section shield tunnel fires using CFD modeling. J. Loss Prev. Process Ind. 44, 158–170.